

1 **CO₂ flux over young and snow-covered Arctic pack ice in**
2 **winter and spring**

3

4 Daiki Nomura^{1, 2, 3, 4*}, Mats A. Granskog⁵, Agneta Fransson⁵, Melissa Chierici^{6, 7}, Anna
5 Silyakova⁸, Kay I. Ohshima^{1, 3}, Lana Cohen⁵, Bruno Delille⁹, Stephen R. Hudson⁵, and
6 Gerhard S. Dieckmann¹⁰

7

8 1 Institute of Low Temperature Science, Hokkaido University, Kita-19, Nishi-8, Kita-
9 ku, Sapporo, Hokkaido 060-0819, Japan.

10

11 2 Faculty of Fisheries Sciences, Hokkaido University, 3-1-1, Minato-cho, Hakodate,
12 Hokkaido 041-8611, Japan.

13

14 3 Arctic Research Center, Hokkaido University, Kita-21, Nishi-11, Kita-ku, Sapporo,
15 Hokkaido 001-0021, Japan.

16

17 4 Global Station for Arctic Research, Global Institution for Collaborative Research and
18 Education, Hokkaido University, Kita-8, Nishi-5, Kita-ku, Sapporo, Hokkaido 060-
19 0808, Japan.

20

21 5 Norwegian Polar Institute, Fram Centre, NO-9296 Tromsø, Norway.

22

23 6 Institute of Marine Research, NO-9294, Tromsø, Norway.

24

25 7 FRAM-High North Research Centre for Climate and the Environment, Tromsø,
26 Norway.

27

28 8 CAGE, Centre for Arctic Gas Hydrate, Environment and Climate, Tromsø, Norway.

29

30 9 Unité d'Océanographie Chimique, Freshwater and Oceanic science Unit of research,
31 Université de Liège, Liège, Belgium.

32

33 10 Alfred Wegener Institute for Polar and Marine Research, Bremerhaven, Germany.

34

35

36 *Corresponding author: Daiki Nomura, e-mail: daiki.nomura@fish.hokudai.ac.jp,

37 Faculty of Fisheries Sciences, Hokkaido University, 3-1-1, Minato-cho, Hakodate,

38 Hokkaido 041-8611, Japan.

39

40

41

42 **Abstract**

43

44 Rare CO₂ flux measurements from Arctic pack ice show that two types of ice contribute
45 to the release of CO₂ from the ice to the atmosphere during winter and spring: young,
46 thin ice with a thin layer of snow, and older (several weeks), thicker ice with thick snow
47 cover. Young, thin sea ice is characterized by high salinity and high porosity, and snow-
48 covered thick ice remains relatively warm ($>-7.5^{\circ}\text{C}$) due to the insulating snow cover
49 despite air temperatures as low as -40°C . Therefore, brine volume fractions of these
50 two ice types are high enough to provide favorable conditions for gas exchange between
51 sea ice and the atmosphere even in mid-winter. Although the potential CO₂ flux from
52 sea ice decreased due to the presence of the snow, the snow surface is still a CO₂ source
53 to the atmosphere for low snow density and thin snow conditions. We found that young
54 sea ice that is formed in leads without snow cover produces CO₂ fluxes an order of
55 magnitude higher than those in snow-covered older ice ($+1.0 \pm 0.6 \text{ mmol C m}^{-2} \text{ day}^{-1}$
56 for young ice, and $+0.2 \pm 0.2 \text{ mmol C m}^{-2} \text{ day}^{-1}$ for older ice).

57

58

59

60 **1 Introduction**

61

62 Arctic sea ice is changing dramatically, with rapid declines in summer sea ice extent
63 and a shift towards younger and thinner first-year ice rather than thick multi-year ice
64 (e.g., Stroeve et al., 2012; Meier et al., 2014; Lindsay and Schweiger, 2015). Although
65 the effects of sea ice formation and melting on biogeochemical cycles in the ocean have
66 previously been discussed (e.g., Vancoppenolle et al., 2013), the effects of sea ice freeze
67 and melt processes on carbon dioxide (CO₂) exchange with the atmosphere are still
68 largely unknown (Parmentier et al., 2013).

69

70 Recent CO₂ flux measurements on sea ice indicate that sea ice is an active component in
71 gas exchange between ocean and atmosphere (Nomura et al., 2013; Geilfus et al., 2013;
72 2014; Delille et al., 2014; Brown et al., 2015; Kotovitch et al., 2016). The sea-ice CO₂
73 fluxes depend on (a) the difference in the partial pressure of CO₂ ($p\text{CO}_2$) between the

74 sea ice surface and air, (b) brine volume fraction at the ice-snow interface, (c) ice
75 surface condition including the snow deposited on ice, and (d) wind-driven pressure
76 pumping through the snow. For (a), it is known that the air-sea ice CO₂ flux is driven
77 by the differences in pCO₂ between the sea ice surface and atmosphere (e.g. Delille et
78 al., 2014; Geilfus et al., 2014). Brine pCO₂ changes due to processes within the sea ice,
79 such as thermodynamic process (e.g., Delille et al., 2014), biological activity (e.g.,
80 Delille et al., 2007; Fransson et al., 2013; Rysgaard et al., 2013), and calcium carbonate
81 (CaCO₃; ikaite) formation and dissolution (e.g., Papadimitriou et al., 2012). When pCO₂
82 in brine is higher than that of air pCO₂, brine has the potential to release CO₂ to the
83 atmosphere. Brine volume fraction (b) controls the permeability of sea ice (Golden et al.
84 1998) and thus CO₂ fluxes (Delille et al. 2014; Geilfus et al 2014). The air-sea ice CO₂
85 flux is also strongly dependent on the sea ice surface conditions (c) (Nomura et al.,
86 2010a, 2013; Geilfus et al., 2013; 2014; Barber et al., 2014; Brown et al., 2015;
87 Fransson et al., 2015). Nomura et al. (2013) proposed that snow properties (e.g., water
88 equivalent) are important factors affecting gas exchange processes on sea ice. In
89 addition, frost flowers (vapor-deposited ice crystals that wick brine from the sea ice
90 surface) promote CO₂ flux from the ice to the atmosphere (Geilfus et al., 2013; Barber
91 et al., 2014; Fransson et al., 2015). Finally, for (d), it is thought that CO₂ flux is affected
92 by wind pumping through the snow pack (Massman et al., 1995; Takagi et al., 2005) in
93 which the magnitude of CO₂ flux through snow or underlying soil (e.g., Takagi et al.,
94 2005) can increase the transport relative to molecular diffusion by up to 40% (Bowling
95 and Massman, 2011). These results were mainly found over land-based snow (soil and
96 forest), and thus they are still poorly understood over sea ice (Papakyriakou and Miller,
97 2011).

98

99 In addition to the processes described above, the CO₂ flux over sea ice may also be
100 influenced by the temperature difference between the ice surface and the atmosphere.
101 This has been shown in previous studies in dry snowpacks over land surfaces. These
102 studies show that there is an unstable air density gradient due to heating at the bottom
103 producing a strong temperature difference between the bottom and top of the snowpack
104 (e.g., Powers et al., 1985; Severinghaus et al., 2010). This produces air flow within the
105 snowpack, which is a potentially significant contributor to mixing and transport of gas

106 and heat within the snowpack. We expect that this process would also occur in snow
107 over sea ice, especially during the wintertime when air temperatures are coldest and the
108 temperature difference between sea ice surface (snow bottom) and atmosphere is largest
109 (e.g., Massom et al., 2001). Generally, the sea ice surface under thick snow cover is
110 warm due to the heat conduction from the bottom of sea ice and the insulating effect of
111 the snow cover, and a strong temperature difference between the sea ice surface and
112 atmosphere is observed (e.g., Massom et al., 2001). Such a temperature difference
113 would produce an unstable air density gradient and upward transport of air containing
114 CO₂ degassed at the sea-ice surface, thereby enhancing CO₂ exchange between sea ice
115 and atmosphere.

116

117 In the ice-covered Arctic Ocean, storm periods which produce high wind speeds and
118 open leads are also important for air-to-sea CO₂ fluxes (Fransson et al., 2017) due to the
119 under-saturation of the surface waters in CO₂ with respect to the atmosphere. In
120 addition, the subsequent ice growth and frost flower formation in open leads promote
121 ice-to-air CO₂ fluxes in winter (e.g. Barber et al., 2014). Given the fact that Arctic sea
122 ice is shrinking and shifting from multi-year ice to first-year ice (e.g., Stroeve et al.,
123 2012; Meier et al., 2014; Lindsay and Schweiger, 2015), the area of open ocean and
124 thinner seasonal ice is increasing. Thus, a potential consequence may be increased
125 contribution of open ocean surface and/or thinner sea ice to the overall CO₂ fluxes of
126 the Arctic Ocean. The dynamics of the thinner ice pack, through formation of leads and
127 new ice, will play an important role in the gas fluxes from the ice pack. However, there
128 is a definite lack of information on sea ice processes during wintertime due to the
129 difficulty in acquiring observations in winter pack ice, as reflected by the fact that most
130 of the previous winter CO₂ flux measurements have been taken over landfast ice.

131

132 The Norwegian young sea ICE (N-ICE2015) campaign in winter and spring 2015
133 provided opportunities to examine CO₂ fluxes between sea ice and atmosphere in a
134 variety of snow and ice conditions in pack ice north of Svalbard. Formation of leads and
135 their rapid refreezing allowed us to examine air–sea ice CO₂ fluxes over thin young sea
136 ice, occasionally covered with frost flowers in addition to the snow-covered older ice
137 that covers most of the pack ice area. The objectives of this study were to understand

138 the effects of i) thin sea ice and frost flower formation on the air–sea ice CO₂ flux in
139 leads, ii) effect of snow-cover on the air–sea ice CO₂ flux over thin, young ice in the
140 Arctic Ocean during winter and spring seasons, and iii) of the effect of the temperature
141 difference between sea ice and atmosphere (including snow cover) on the air–sea ice
142 CO₂ flux.

143

144

145 **2 Materials and Methods**

146

147 **2.1 Study area**

148

149 This study was performed during N-ICE2015 campaign with R/V Lance in the pack ice
150 north of Svalbard from January to June 2015 (Granskog et al., 2016). Air–sea ice CO₂
151 flux measurements were carried out from January to May 2015 during the drift of floes
152 1, 2, and 3 of the N-ICE2015 campaign (Figures 1 and 2, Table 1). The ice pack was a
153 mixture of young ice, first-year ice and second-year ice (Granskog et al., 2017), and
154 both the first- and second-year ice had a thick snow cover (Merkouriadi et al., 2017;
155 Rösel et al., 2018). Air–sea ice CO₂ flux measurements were made over young ice (YI
156 stations), first-year ice (FI stations), and old ice (multi-year ice) (OI station). In the N-
157 ICE2015 study region, the modal ice thickness was about 1.3–1.5 m and the modal
158 snow thickness was about 0.5 m (Rösel et al., 2018). Formation of leads and their rapid
159 refreezing provided us the opportunity to examine air–sea ice CO₂ fluxes over thin sea
160 ice, occasionally covered with frost flowers at station YI1 (Figure 2 and Table 1). Air
161 temperature and wind speed were measured at a 10 m weather mast on the ice floe
162 installed about 400 m away from R/V Lance (Cohen et al., 2017).

163

164

165 **2.2 CO₂ flux measurements**

166

167 The air–sea ice CO₂ flux was measured with LI-COR 8100-104 chambers connected to
168 a LI-8100A soil CO₂ flux system (LI-COR Inc., USA) (Figure 2). This enclosed
169 chamber method has been widely applied over snow and sea ice (e.g., Schindlbacher et

170 al., 2007, Geilfus et al., 2015). Two chambers were connected in a closed loop to the
171 infrared gas analyzer (LI-8100A, LI-COR Inc., USA) to measure CO₂ concentration
172 through the multiplexer (LI-8150, LI-COR Inc., USA) with an air pump rate at 3 L min⁻¹.
173 ¹. Power was supplied by a car battery (8012-254, Optima Batteries Inc., USA). Four
174 CO₂ standards (324–406 ppmv) traceable to the WMO scale (Inoue and Ishii, 2005)
175 were prepared to calibrate the CO₂ gas analyzer prior to the observations. CO₂ flux was
176 measured in the morning or in the afternoon during low-wind conditions (Table 2), to
177 minimize the effect of wind on the flux (Bain et al., 2005).

178

179 One chamber was installed over undisturbed snow or frost flowers on the ice surface.
180 The chamber collar was inserted 5 cm into the snow and 1 cm into ice at the frost flower
181 site to avoid air leaks between the inside and outside of the chamber. The second
182 chamber was installed on bulk sea ice after removing the snow or frost flowers. Flux
183 measurements were begun immediately in order to minimize the changes of the ice
184 surface condition. In order to evaluate the effect of removing snow on the ice surface
185 temperature, temperature was monitored during CO₂ flux measurements at station FI6.
186 A temperature sensor (RTR 52, T & D Corp., Japan) was installed in the top of the ice
187 (1 cm) surface after snow removal. During the first CO₂ flux measurements (about 30
188 minutes), the ice surface temperature was stable at -5.8°C, suggesting that the effect of
189 removing snow on the variation of sea ice surface temperature was negligible within 30
190 minutes. The ice surface temperature decreased from -5.8°C to -8.0°C at 200 minutes
191 after removal of snow. Therefore, in this paper, the data of the initial 30 minutes of CO₂
192 flux measurement after removal of snow or frost flowers was used. The chamber was
193 closed for 20 minutes in a sequence. The 20-minute time period was used because CO₂
194 fluxes over sea ice are much smaller than over land. The CO₂ concentrations within the
195 chamber were monitored to ensure that they changed linearly throughout the
196 measurement period (example given in Figure 3). The CO₂ flux (mmol C m⁻² day⁻¹)
197 (positive value indicates CO₂ being released from ice surface to air) was calculated
198 based on the changes of the CO₂ concentration within the headspace of the chamber
199 with LI-COR software (Model: LI8100PC Client v.3.0.1.). The mean coefficient of
200 variation for CO₂ flux measurements was less than 3.0% for CO₂ flux values larger than
201 ±0.1 mmol C m⁻² day⁻¹. For CO₂ flux values smaller than ±0.1 mmol C m⁻² day⁻¹, the

202 mean coefficient of variation for CO₂ flux measurements was higher than 3.0%,
203 suggesting that the detection limit of this system is about 0.1 mmol C m⁻² day⁻¹.

204

205 In this paper, we express the CO₂ flux measured over the snow and frost flowers as
206 F_{snow} and F_{ff}, respectively. The flux measured directly over the sea ice surface either on
207 snow-free ice or after removal of snow and frost flowers as F_{ice}. F_{snow} and F_{ff} are the
208 natural flux (snow and frost flowers are part of the natural system), and F_{ice} is the
209 potential flux in cases when snow or frost flowers are removed. While removal of snow
210 and frost flowers is an artificial situation, comparisons between F_{ice} and F_{snow} or F_{ff}
211 provide information about the effect of snow and frost flowers on the CO₂ flux.
212 Therefore, in this study, we examine both situations for CO₂ flux.

213

214

215 **2.3 Sampling of snow, frost flowers, brine, and sea ice**

216

217 For salinity measurements, separate samples were taken for snow only, snow and frost
218 flowers, and sea ice surface scrapes. The samples were taken using a plastic shovel,
219 placed into plastic bags and stored in an insulated box for transport to the ship-lab for
220 further processing. Samples were melted slowly (2–3 days) in the dark at +4°C. The
221 temperature of the snow and frost flower samples were measured during CO₂ flux
222 measurements (approximately 60 minutes after the onset of the CO₂ flux measurement)
223 using a needle-type temperature sensor (Testo 110 NTC, Brandt Instruments, Inc.,
224 USA). The accuracy of this sensor is ±0.2°C. Snow density was obtained using a fixed
225 volume sampler (Climate Engineering, Japan) and weight measurement. The depth of
226 the snow pack and frost flowers was also recorded using a ruler.

227

228 Brine was also collected at stations FI3–6 for salinity, dissolved inorganic carbon (DIC)
229 and total alkalinity (TA) measurements. Brine was collected from sackholes as
230 described in Gleitz et al. (1995). The sackholes were drilled using a 9 cm diameter ice
231 corer (Mark II coring system, Kovacs Enterprises, Inc., USA) to a depth of 30 cm. The
232 sackholes were then covered with a lid of 5 cm-thick urethane to reduce heat and gas
233 transfer between brine and atmosphere. When brine accumulated at the bottom of the

234 sackholes (approximately 15 minutes), it was collected with a plastic syringe (AS ONE
235 Corporation, Japan) and kept in 500 mL unbreakable plastic bottles (I-Boy, AS ONE
236 Corporation, Japan) in order to facilitate safe transport to the sampling sites in cold and
237 harsh conditions. The brine bottles were filled without head-space and immediately
238 stored in an insulated box to prevent freezing. Immediately after return to the ship, the
239 brine samples were transferred to 250 mL borosilicate bottles (DURAN Group GmbH,
240 Germany) for DIC and TA measurements using tubing to prevent contact with air. The
241 samples were preserved with saturated mercuric chloride (HgCl_2 , 60 μL for a 250 mL
242 sample) and stored in the dark at $+10^\circ\text{C}$ until analyses was performed at the Institute of
243 Marine Research, Norway.

244

245 Sea ice was collected by the same ice corer as described for brine collection and at the
246 same location as snow and frost flowers were collected. Sea ice temperature was
247 measured by the same sensor as described for snow. For the ice cores, the temperature
248 sensor was inserted in small holes drilled into the core. The core was then cut with a
249 stainless steel saw into 10 cm sections and stored in plastic bags for subsequent salinity
250 measurements. The ice core sections were kept at $+4^\circ\text{C}$ and melted in the dark prior to
251 measurement.

252

253

254 **2.4 Sample analysis**

255

256 Salinities for melted snow, frost flowers, sea ice, and brine were measured with a
257 conductivity sensor (Cond 315i, WTW GmbH, Germany). For calibration of salinity
258 measurement, a Guildline PORTASAL salinometer Model 8410A, standardized by
259 International Association for the Physical Sciences of the Oceans (IAPSO) standard
260 seawater (Ocean Scientific International Ltd, UK) was used. The accuracy of this sensor
261 was ± 0.003 .

262

263 Analytical methods for DIC and TA determination are fully described in Dickson et al.
264 (2007). DIC in brine was determined using gas extraction of acidified sample followed
265 by coulometric titration and photometric detection using a Versatile INstrument for the

266 Determination of Total inorganic carbon and titration Alkalinity (VINDTA 3C,
267 Germany). TA of brine was determined by potentiometric titration of 40 mL sample in
268 open cell with 0.05 N hydrochloric acid using a Titrino system (Metrohm, Switzerland).
269 The average standard deviation for DIC and TA, determined from replicate sample
270 analyses from one sample, was within $\pm 2 \mu\text{mol kg}^{-1}$ for both DIC and TA. The accuracy
271 of the DIC and TA measurements were $\pm 2 \mu\text{mol kg}^{-1}$ for both DIC and TA, as
272 estimated using Certified Reference Materials (CRM, provided by A. G. Dickson,
273 Scripps Institution of Oceanography, USA). The pCO_2 of brine ($\text{pCO}_{2\text{b}}$) was derived
274 from in situ temperature, salinity, DIC and TA of brine using the carbonate speciation
275 program CO2SYS (Pierrot et al., 2006). The calculated $\text{pCO}_{2\text{b}}$ values (Table 2) varied
276 within 1.7% when DIC and TA values were changed within the standard deviation (± 2
277 $\mu\text{mol kg}^{-1}$). We used the carbonate dissociation constants (K_1 and K_2) of Mehrbach et al.
278 (1973) as refit by Dickson and Millero (1987), and the KSO_4 determined by Dickson
279 (1990). The conditional stability constants used to derive pCO_2 are only valid for
280 temperatures above 0°C and salinities between 5 and 50. Studies in spring ice indicated
281 that seawater thermodynamic relationships may be acceptable in warm and low-salinity
282 sea ice (Delille et al., 2007). In sea ice brines at even moderate brine salinities of 80,
283 Brown et al. (2014) found that measured and calculated values of the CO_2 system
284 parameters can differ by as much as 40%. On the other hand, because the CO_2 system
285 parameters are much more variable in sea ice than in seawater, sea ice measurements
286 demand less precision than those in seawater. Fransson et al. (2015) performed one of
287 the few detailed analyses of the internal consistency using four sets of dissociation
288 constants and found that the deviation between measured and calculated DIC varied
289 between ± 6 and $\pm 11 \mu\text{mol kg}^{-1}$, respectively. This error in calculated DIC was
290 considered insignificant in relation to the natural variability in sea ice.

291

292 The pCO_2 of atmosphere was calculated from CO_2 concentration (ppmv) at Ny-Ålesund,
293 Svalbard (<http://www.esrl.noaa.gov/gmd/dv/iadv/>) taking into account saturated water
294 vapor and atmospheric pressure during sampling day.

295

296 The water equivalent was computed for snow by multiplying snow thickness by snow
297 density (Jonas et al., 2009). Brine volume of sea ice was calculated from the

298 temperature and salinity of sea ice according to Cox and Weeks (1983) and Petrich and
299 Eicken (2010).

300

301

302 **3 Results**

303

304 **3.1 Air temperature**

305

306 Air temperature is shown in Figure 4. During the study period, the air temperature
307 varied considerably from a low of -41.3°C (30 January) to a high of $+1.7^{\circ}\text{C}$ (15 June)
308 (Hudson et al., 2015). Even in wintertime (from January to March), rapid increases of
309 air temperature from less than -30°C up to -0.2°C (e.g., 18 February), were observed.
310 In springtime (from April to June), the air temperature increased continuously, and from
311 1 June, air temperatures were near 0°C , although rapid increases (and subsequent
312 decreases) of air temperature to near 0°C were observed on two occasions in mid-May
313 (Cohen et al., 2017).

314

315

316 **3.2 Characteristics of snow, sea ice, and frost flowers**

317

318 The snow and ice thickness at the observation sites ranged between 0.0 and 60.0 cm and
319 between 15.0 and >200 cm, respectively (Table 1). The thin snow and ice represent
320 newly formed ice in leads at station YI1. The thickness of the frost flowers ranged from
321 1.0 to 2.5 cm.

322

323 Figure 5 shows vertical profiles of snow and ice temperature and salinity in the top 20
324 cm of ice. Temperatures within the snowpack depended on the air temperature at the
325 time of observation. However, the bottom of the snow and the surface of the sea ice
326 were relatively warm ($T > -7.5^{\circ}\text{C}$), except for the frost flower station YI1 and the multi-
327 year ice station OI1 (Figure 5a and Table 2). High salinities ($S > 18.6$) characterized the
328 bottom of the snow and the surface of the sea ice, except for the multi-year ice station
329 OI1 (Figure 5b). At the multi-year ice station OI1, salinity was zero through the snow

330 and top of sea ice. Salinity of frost flowers was up to 92.8 for the thin ice station YI1
331 (Figure 5b). Snow density and water equivalent ranged from 268 to 400 kg m⁻³ and 11
332 to 180 kg m⁻², respectively (Table 2).

333

334

335 **3.3 Physical and chemical properties of brine**

336

337 The brine volume fraction, temperature, salinity, DIC, TA, and calculated pCO₂ are
338 summarized in Table 2. Brine volume fraction in the top 20 cm of ice was between 9 to
339 17%, except for the value of 0% at the multi-year ice station OI1 (Table 2). Brine
340 temperatures and salinity ranged from -5.3 to -3.3°C and 51.8 to 86.6, respectively.
341 DIC and TA of brine ranged from 3261 to 4841 μmol kg⁻¹ and 3518 to 5539 μmol kg⁻¹,
342 respectively. The pCO₂ of brine (pCO_{2 b}) (334–693 μatm) was generally higher than
343 that of atmosphere (pCO_{2 a}) (401 ± 7 μatm), except for station FI4.

344

345

346 **3.4 CO₂ flux**

347

348 Table 3 summarizes the CO₂ flux measurements for each surface condition. For
349 undisturbed natural surface conditions, i.e. measurements directly on the snow surface
350 (F_{snow}) or the frost flowers (F_{ff}) on young ice, the mean CO₂ flux was +0.2 ± 0.2 mmol
351 C m⁻² day⁻¹ for F_{snow} and +1.0 ± 0.6 mmol C m⁻² day⁻¹ for F_{ff}. The potential flux in
352 cases when snow or frost flowers had been removed (F_{ice}) was +2.5 ± 4.3 mmol C m⁻²
353 day⁻¹. The air–sea ice CO₂ fluxes measured over the ice surface (F_{ice}) increased with
354 increasing differences in pCO₂ between brine and atmosphere (ΔpCO_{2 b-a}) with
355 significant correlation (R² = 0.9, p < 0.02), but this was not the case for F_{snow} (R² = 0.0,
356 p < 0.96) (Figure 6).

357

358

359

360 **4 Discussion**

361

362 4.1 Effect of snow cover on the physical properties of sea ice surface

363

364 In this study, we examined CO₂ fluxes between the sea ice and atmosphere in a wide
365 range of air temperatures and diverse snow and ice conditions (Table 2). The bottom of
366 the snow pack and the surface of the sea ice remained relatively warm ($>-7.5^{\circ}\text{C}$)
367 (Figure 5a, Table 2), except for stations OI1 and YI1, even though air temperature was
368 sometimes below -40°C (Figure 4). Relatively warm ice temperatures were likely due
369 to the upward heat transport from the bottom of the ice and in some cases the thick
370 insulating snow cover, except for stations OI1 and YI1 (Table 2). Therefore, snow acted
371 as thermal insulator over sea ice, and in general the snow depths observed during N-
372 ICE2015 point towards this being representative for first-year and second-year or older
373 ice in the study region in winter 2015 (Rösel et al., 2018). The young and first-year ice
374 surfaces were characterized by high salinities (Figure 5b). During sea ice formation,
375 upward brine transport to the snow pack occurs (e.g., Toyota et al., 2011). In addition,
376 brine within the sea ice was not completely drained as compared to that of multi-year
377 ice. Furthermore, formation of frost flowers and subsequent wicking up of surface brine
378 into the frost flowers also provides high salinity at the surface of sea ice (Kaleschke et
379 al., 2004; Geilfus et al., 2013; Barber et al., 2014; Fransson et al., 2015) as observed in
380 this study ($S>92$) (Figure 5b). Snowfall over the frost flowers would have preserved the
381 high salinity at the bottom of snow pack and top of sea ice for young and first-year ice.

382

383 As a result of the combination of the relatively high temperature and high salinity at the
384 top of sea ice, brine volume fractions in the upper parts of the sea ice were high, up to
385 17% (Table 2). It has been shown that ice permeability increases by an order of
386 magnitude when brine volume fraction is greater than 5% as compared to when the
387 brine volume fraction is less than 5% (Golden et al., 1998; Pringle et al., 2009; Zhou et
388 al., 2013). A brine volume fraction of 5% would correspond to a temperature of -5°C
389 for a bulk ice salinity of 5 – the so called “law of fives” (Golden et al., 1998). Because
390 sea ice temperatures are low, thereby reducing the permeability in winter season, air–
391 sea ice CO₂ flux is generally at its minimum in the winter (e.g., Delille et al., 2014).
392 However, in our study, the brine volume fractions were generally $>9\%$, except for
393 station OI1 with fresh ice at the surface, providing conditions for active gas exchange

394 within sea ice and between sea ice and atmosphere. This situation was likely made
395 possible due to the thick snow cover and relatively thin and young sea ice.

396

397

398 **4.2 CO₂ fluxes over different sea-ice surface types**

399

400 The CO₂ flux measurements over different surface conditions indicate that the snow
401 cover over sea ice affects the magnitude of air–sea ice CO₂ flux, especially for stations
402 FI5 and FI6 (Table 3). For undisturbed natural surface conditions, the CO₂ flux
403 measured directly over snow-covered first-year ice and young ice with frost flowers
404 (F_{snow} and F_{ff}) was lower in magnitude than that for potential flux obtained directly over
405 the ice surface after removing snow (F_{ice}) for stations FI5, FI6, and YI1.

406

407 F_{ff} indicates that the frost flower surface on young thin ice is a CO₂ source to the
408 atmosphere and F_{ff} was higher than F_{snow} , except for station FI1. This finding was
409 consistent with the previous studies (Geilfus et al., 2013; Barber et al., 2014; Fransson
410 et al., 2015). At multi-year ice station OI1, neither snow or ice surface acted as a CO₂
411 source/sink. The surface of multi-year ice did not contain any brine (Figure 5b and
412 Table 2), and the top of the ice was clear, colorless and very hard, suggesting
413 superimposed formation at the top of sea ice. This situation would be similar as for
414 freshwater-ice and superimposed-ice as these non-porous media block gas exchange
415 effectively at the sea ice surface (Delille et al., 2014). Snow-ice and superimposed-ice
416 were frequently found in second-year ice cores during N-ICE2015 (Granskog et al.,
417 2017), so the ‘blocking’ of gas exchange in second-year and multi-year ice may be a
418 widespread process in the Arctic.

419

420 The magnitude of positive F_{snow} is less than F_{ice} for stations FI5 and FI6 (Table 3)
421 indicating that the potential CO₂ flux from sea ice decreased due to the presence of
422 snow. Previous studies have shown that snow accumulation over sea ice effectively
423 impedes CO₂ exchange (Nomura et al., 2013; Brown et al., 2015). Nomura et al. (2013)
424 reported that 50–90% of the potential CO₂ flux was reduced due to the presence of
425 snow/superimposed-ice at the water equivalent of 57–400 kg m⁻², indicating that the

426 snow properties are an important factor that controls the CO₂ exchange through a
427 snowpack. Comparisons between stations FI5 and FI6 for $F_{\text{snow}}/F_{\text{ice}}$ ratio (0.23 for FI5
428 and 0.02 for FI6) and water equivalent (11 kg m⁻² for FI5 and 127 kg m⁻² for FI6)
429 indicate that the potential CO₂ flux is reduced (80% for FI5 and 98% for FI6 of the
430 potential CO₂ flux) with increasing water equivalent. Although the magnitude of the
431 potential CO₂ flux through the sea ice surface decreased by the presence of snow for
432 stations FI5 and FI6 (Table 3), the snow surface still presents a CO₂ source to the
433 atmosphere for low snow density and shallow depth conditions (e.g., +0.6 mmol C m⁻²
434 day⁻¹ for FI5).

435

436 For F_{ice} , there were negative CO₂ fluxes at stations FI3 and FI4 (-0.6 mmol C m⁻² day⁻¹
437 for FI3 and -0.8 mmol C m⁻² day⁻¹ for FI4) (Table 3). These fluxes corresponded to low
438 or negative $\Delta p\text{CO}_2_{\text{b-a}}$ (Table 2 and Figure 6). Negative CO₂ fluxes should correspond to
439 negative $\Delta p\text{CO}_2_{\text{b-a}}$. Therefore, the uncertainty for the calculation of carbonate
440 chemistry may be one reason for the discrepancy in pCO₂ calculation at station FI3
441 (Brown et al., 2014).

442

443

444 **4.3 Comparison to earlier studies on sea-ice to air CO₂ flux**

445

446 The CO₂ fluxes measured over the undisturbed natural surface conditions (F_{snow} and F_{ff})
447 in this study ranged from +0.1 to +1.6 mmol C m⁻² day⁻¹ (Table 3), which are at the
448 lower end of the reported range based on the chamber method and eddy covariance
449 method for natural and artificial sea ice (-259.2 to +74.3 mmol C m⁻² day⁻¹)
450 (Zemmelink et al., 2006; Nomura et al., 2006, 2010a, 2010b, 2013; Miller et al., 2011;
451 Papakyriakou and Miller, 2011; Geilfus et al., 2012, 2013, 2014; Barber et al., 2014;
452 Delille et al., 2014; Sørensen et al., 2014; Brown et al., 2015; Kotovitch et al., 2016).
453 Direct comparison to these previous studies is complicated because CO₂ flux
454 measurements with both chamber and eddy covariance techniques were used during
455 different conditions and ice surface characteristics. In addition, discrepancies between
456 chamber and eddy covariance measurements of air-ice CO₂ fluxes have been repeatedly
457 observed. The footprint size of CO₂ exchange measured with the two approaches

458 (Zemmelink et al., 2006, 2008; Burba et al., 2008; Amiro, 2010; Miller et al., 2011;
459 Papakyriakou and Miller, 2011; Sørensen et al., 2014; Miller et al., 2015) may be one
460 reason for the large difference. The eddy covariance method reflects a flux integrated
461 over a large area that can contain several different surface types. Therefore, eddy-
462 covariance appears to be more useful for understanding fluxes at large spatial and
463 temporal scales. On the other hand, the chamber method reflects the area where
464 chamber was covered, and it is useful for understanding the relationship between fluxes
465 and ice surface conditions on smaller scales. The different spatial scales of the two
466 methods may be therefore one reason for the discrepancy in CO₂ flux measurements.

467

468 Comparison of the natural CO₂ flux range (+0.1 to +1.6 mmol C m⁻² day⁻¹ for F_{snow} and
469 F_{ff}) (Table 3) with previous estimates derived from the chamber method (-5.2 to +6.7
470 mmol C m⁻² day⁻¹) (Nomura et al., 2006, 2010a, 2010b, 2013; Geilfus et al., 2012,
471 2013; 2014; Barber et al., 2014; Delille et al., 2014; Brown et al., 2015; Kotovitch et al.,
472 2016) (these studies include both natural and potential fluxes) shows that CO₂ fluxes
473 during the N-ICE2015 experiment are at the lower end of positive values. However, our
474 potential CO₂ flux (F_{ice}) was a larger CO₂ source (up to +11.8 mmol C m⁻² day⁻¹) than
475 reported in previous studies (+6.7 mmol C m⁻² day⁻¹). In our study, the maximum
476 potential flux (+11.8 mmol C m⁻² day⁻¹) was obtained for F_{ice} at station FI6 (Table 3).
477 In this situation, ΔpCO_{2 b-a} (293 μatm) was the highest (Table 2 and Figure 6), and it is
478 reasonable to consider this as the highest magnitude of positive CO₂ flux within our
479 study. However, a previous study by closed chamber method showed that even for a
480 similar ΔpCO_{2 b-a} (297 μatm) and brine volume fraction (10–15%), the CO₂ flux was
481 +0.7 mmol C m⁻² day⁻¹ for artificial sea ice with no snow in the tank experiment
482 (Nomura et al., 2006).

483

484 The CO₂ flux between the sea ice and overlying air can be expressed by the following
485 equation,

486

$$487 F_{\text{CO}_2} = r_b k \alpha \Delta p\text{CO}_{2 \text{ b-a}},$$

488

489 where r_b is the ratio of surface of the brine channel to sea ice surface, and we assume
490 that the value of r_b is equal to brine volume fraction, k is the gas transfer velocity, α is
491 the solubility of CO_2 (Weiss, 1974), and $\Delta p\text{CO}_2_{b-a}$ is the difference in $p\text{CO}_2$ between
492 brine and atmosphere. The equation is based on the fact that CO_2 transfer between
493 seawater and air is controlled by processes in the near-surface water (Liss, 1973). The
494 gas transfer velocity (k) calculated from F , r_b , α and $\Delta p\text{CO}_2_{b-a}$ was 5.12 m day^{-1} for F_{ice}
495 at station FI6 and 0.29 m day^{-1} for the tank experiment examined in Nomura et al.
496 (2006). This result clearly indicates that the gas transfer velocity for F_{ice} at station FI6 is
497 higher than that of tank experiment examined in Nomura et al. (2006) even with very
498 similar $\Delta p\text{CO}_2_{b-a}$ and brine volume fraction.

499

500 Here, we surmise that the gas transfer velocity and thereby CO_2 flux is greatly enhanced
501 by the temperature difference between sea ice surface and atmosphere. Previous studies
502 indicate that there is an unstable air density gradient in a dry snowpack due to basal
503 heating and the strong temperature difference develops between bottom and top of snow
504 (e.g., Powers et al., 1985; Severinghaus et al., 2010), which enhances the flow of air
505 through the snowpack. We propose that the mixing and transport of gas within the
506 snowpack could also occur over sea ice. Because temperatures at the bottom of snow
507 and the top of sea ice were relatively warm due to a thick insulating snow over sea ice,
508 there was a strong temperature difference between sea ice surface and atmosphere when
509 air temperature was low (Figure 5a and Table 2). For station FI6, the temperature
510 difference between the sea ice surface and atmosphere was 20.2°C after snow removal.
511 On the other hand, in the tank experiment by Nomura et al. (2006), the temperature
512 difference between sea ice surface (top 1.5 cm) and air in the headspace was only 4.5°C .

513

514 Figure 6 shows the relationship between mean air–sea ice CO_2 fluxes and temperature
515 difference between ice and atmosphere. The strong dependence of CO_2 flux with
516 temperature difference ($T_{\text{ice}}-T_a$) was observed, especially for F_{ff} and F_{ice} ($R^2 > 0.7$, $p <$
517 0.01 , linear fitting) (Figure 6). Due to the high brine volume fractions (Table 2), the sea
518 ice surface had enough permeability for gas exchange. In addition, ice temperatures
519 were similar for young and first-year ice (Table 2), indicating that $p\text{CO}_2$ at the top of the

520 sea ice and CO₂ flux would be of similar order of magnitude if thermodynamic
521 processes dominated. Therefore, our results suggest that the CO₂ fluxes even over the
522 frost flowers as a natural condition, would be enhanced by the upward transport of air
523 containing high CO₂ from the surface of sea ice to the atmosphere due to the strong
524 temperature difference between sea ice surface and atmosphere. Although the presence
525 of snow on sea ice has potential to produce a larger temperature difference between sea
526 ice surface and atmosphere and promote the upward transport, the magnitude of the CO₂
527 flux decreased due to the presence of snow. However, for young sea ice with frost
528 flowers (e.g., station Y11), ice surface temperature was warm (Table 2), suggesting that
529 CO₂ flux would be enhanced by the large temperature difference between sea ice
530 surface and atmosphere.

531

532

533

534 **5 Conclusions**

535

536 We measured CO₂ fluxes along with sea ice and snow physical and chemical properties
537 over first-year and young sea ice north of Svalbard in the Arctic pack ice. Our results
538 suggest that young thin snow-free ice, with or without frost flowers, is a source of
539 atmospheric CO₂ due to the high pCO₂ and salinity and relatively high sea ice
540 temperature. Although the potential CO₂ flux from the sea ice surface decreased due to
541 the presence of snow, the snow surface still presents a modest CO₂ source to the
542 atmosphere for low snow density and shallow depth situations. The highest ice-to-air
543 fluxes were observed over thin young sea ice formed in leads. During N-ICE2015 the
544 ice pack was dynamic, and formation of open water was associated with storms, where
545 new ice was formed. The subsequent ice growth in these leads is especially important
546 for the ice-to-air CO₂ fluxes in winter since the flux from young ice is an order of
547 magnitude larger than from snow-covered first-year and older ice.

548

549

550

551 **6 Data availability**

552

553 Data used in this paper will be available at Norwegian Polar Data Centre
554 (data.npolar.no).

555

556

557

558 **7 Acknowledgments**

559

560 We would like to express heartfelt thanks to the crew of R/V Lance and all members of
561 the N-ICE2015 expedition for their support in conducting the field work. This work was
562 supported by the Japan Society for the Promotion of Science (#15K16135, #24-4175),
563 Research Council of Norway (KLIMAFORSK programme, grant 240639), the Centre
564 of Ice, Climate and Ecosystems (ICE) at the Norwegian Polar Institute through the N-
565 ICE project, the Ministry of Climate and Environment and the Ministry of Foreign
566 Affairs of Norway, the Grant for Joint Research Program of the Institute of Low
567 Temperature Science, Hokkaido University and the Grant for Arctic Challenge for
568 Sustainability. AF, MC and MAG were supported by the flagship research program
569 "Ocean acidification and ecosystem effects in Northern waters" within the FRAM-High
570 North Research Centre for Climate and the Environment. BD is a research associate of
571 the F.R.S-FNRS.

572

573

574

575 **Reference list**

576

577 Amiro, B.: Estimating annual carbon dioxide eddy fluxes using open-path analysers for
578 cold forest sites. *Agr. Forest Meteorol.*, 150, 15, 1366–1372. 2010.

579

580 Bain, W. G., Hutyra, L., Patterson, D. C., Bright, A. V., Daube, B. C. Munger, J. W.,
581 Wofsy, S. C.: Wind-induced error in the measurement of soil respiration using closed
582 dynamic chambers. *Agricul. Forest Meteo.*, 131, 3–4, 225–232, 2005.

583

584 Barber, D. G., Ehn, J. K., Pućko, M., Rysgaard, S., Deming, J. W. and co-authors: Frost
585 flowers on young Arctic sea ice: The climatic, chemical and microbial significance of
586 an emerging ice type. *J Geophys. Res.-Atmos.* doi: 10.1002/2014JD021736. 2014.
587

588 Brown, K. A, Miller, L. A., Davelaar, M., Francois, R., and Tortell P. D.: Over-
589 determination of the carbonate system in natural sea ice brine and assessment of
590 carbonic acid dissociation constants under low temperature, high salinity conditions.
591 *Mar. Chem* 165: 36–45. doi: 10.1016/j.marchem.2014.07.005. 2014.
592

593 Brown, K. A., Miller, L.A., Mundy, C. J., Papakyriakou, T., Francois, R., and co-
594 authors: Inorganic carbon system dynamics in landfast Arctic sea ice during the early-
595 melt period. *J. Geophys. Res. Oceans*, 120, 3542–3566.
596 <http://dx.doi.org/10.1002/2014JC010620>. 2015.
597

598 Burba, G., McDermitt, D., Grelle, A., Anderson, D., and Xu, L.: Addressing the
599 influence of instrument surface heat exchange on the measurements of CO₂ flux from
600 open-path gas analyzers, *Global Change Biol.*, 14, 8, 1854–1876, 2008.
601

602 Cohen, L., Hudson, S. R., Walden, V. P., Graham, R. M., and Granskog, M. A.:
603 Meteorological conditions in a thinner Arctic sea ice regime from winter through
604 summer during the Norwegian young sea ICE expedition (N-ICE2015), *J. Geophys. Res.*
605 *Atmos.*, 122, 7235–7259, doi:10.1002/2016JD026034, 2017.
606

607 Cox, G. F. N., and Weeks W. F.: Equations for determining the gas and brine volumes
608 in sea-ice samples, *J. Glaciol.*, 29, 306–316, 1983.
609

610 Delille, B., Jourdain, B., Borges, A. V., Tison, J.-L., and Delille, D.: Biogas (CO₂, O₂,
611 dimethylsulfide) dynamics in spring Antarctic fast ice, *Limnol. Oceanogr.*, 52, 1367–
612 1379, 2007.
613

614 Delille, B., Vancoppenolle, M., Geilfus, N.-X., Tilbrook, B., Lannuzel, D., and co-
615 authors: Southern Ocean CO₂ sink: the contribution of the sea ice, *J. Geophys. Res.*
616 *Oceans*. 119 (9), 6340–6355, 2014.

617

618 Dickson, A. G., and Millero F. J.: A comparison of the equilibrium constants for the
619 dissociation of carbonic acid in seawater media, *Deep-Sea Res.* 34, 1733–1743, 1987.

620

621 Dickson, A. G.: Thermodynamics of the dissociation of boric acid in synthetic seawater
622 from 273.15 to 318.15 K, *Deep-Sea Res.* 37, 755–766, 1990.

623

624 Dickson, A. G., Sabine, C. L., and Christian, J. R. Eds.: *Guide to Best Practices for*
625 *Ocean CO₂ Measurements*, PICES Special Publication, 3, 191 pp, 2007.

626

627 Fransson, A., Chierici, M., Miller, L. A., Carnat, G., Thomas, H., and co-authors:
628 Impact of sea ice processes on the carbonate system and ocean acidification state at the
629 ice-water interface of the Amundsen Gulf, Arctic Ocean, *J. Geophys. Res.*, 118, 1–23,
630 doi:10.1002/2013JC009164, 2013.

631

632 Fransson, A., Chierici, M., Abrahamsson, K., Andersson, M., Granfors, A., and co-
633 authors: CO₂-system development in young sea ice and CO₂ gas exchange at the ice/air
634 interface mediated by brine and frost flowers in Kongsfjorden, Spitsbergen, *Ann.*
635 *Glaciol.*, 56, 69, doi: 10.3189/2015A0G69A563, 2015.

636

637 Fransson, A., Chierici, M., Skjelvan, I., Olsen, A., Assmy, P., Peterson, A. K., Ward,
638 B.: Effects of sea-ice and biogeochemical processes and storms on under-ice water f
639 CO₂ during the winter-spring transition in the high Arctic Ocean: Implications for sea-
640 air CO₂ fluxes, *J. Geophys. Res. Oceans*, 122(7), 5566–5587.
641 <https://doi.org/10.1002/2016JC012478>. 2017.

642

643 Geilfus, N.-X., Carnat, G., Papakyriakou, T., Tison, J.-L., Else, B. and co-authors:
644 Dynamics of pCO₂ and related air–ice CO₂ fluxes in the Arctic coastal zone (Amundsen
645 Gulf, Beaufort Sea), *J. Geophys. Res.*, 117, C00G10, doi:10.1029/2011JC007118, 2012.

646
647 Geilfus, N.-X., Carnat, G., Dieckmann, G. S., Halden, N., Nehrke, G., and co-authors:
648 First estimates of the contribution of CaCO₃ precipitation to the release of CO₂ to the
649 atmosphere during young sea ice growth, *J. Geophys. Res.*, 118:244–255.
650 <http://dx.doi.org/10.1029/2012JC007980>, 2013.
651
652 Geilfus, N.-X., Tison, J.-L., Ackley, S. F., Galley, R. J., Rysgaard, S., and co-authors:
653 Sea ice pCO₂ dynamics and air–ice CO₂ fluxes during the Sea Ice Mass Balance in the
654 Antarc-tic (SIMBA) experiment – Bellingshausen Sea, Antarctica, *The Cryosphere*, 8,
655 2395–2407, doi:10.5194/tc-8-2395-2014, 2014.
656
657 Geilfus, N.-X., Galley, R. J., Crabeck, O., Papakyriakou, T., Landy, J., Tison, J.-L. and
658 Rysgaard, S.: Inorganic carbon dynamics of melt-pond-covered first-year sea ice in the
659 Canadian Arctic, *Biogeosci.*, 12, 2047–2061, doi:10.5194/bg-12-2047-2015, 2015.
660
661 Gleitz, M., Vonderlo, M. R., Tomas, D. N., Dieckmann, G. S. and Millero F. J.:
662 Comparison of summer and winter inorganic carbon, oxygen and nutrient
663 concentrations in Antarctic sea ice brine, *Mar. Chem.*, 51, 81–89, 1995.
664
665 Golden, K. M., Ackley, S. F. and Lytle, V. I.: The percolation phase transition in sea ice,
666 *Science*, 282, 2238–2241, 1998.
667
668 Granskog, M. A., Assmy, P., Gerland, S., Spreen, G., Steen, H., and co-authors: Arctic
669 research on thin ice: Consequences of Arctic sea ice loss, *Eos Transactions AGU*, 97,
670 22–26, doi:10.1029/2016EO044097, 2016.
671
672 Granskog, M. A., Rösel, A., Dodd, P. A., Divine, D., Gerland, S., and co-authors: Snow
673 contribution to first-year and second-year Arctic sea ice mass balance north of Svalbard,
674 *J. Geophys. Res. Oceans*, 122, 2539-2549, doi: 10.1002/2016JC012398, 2017.
675
676 Hudson, S. R., Cohen, L., and Walden, V.: N-ICE2015 surface meteorology (Data set),
677 Norwegian Polar Institute, doi: 10.21334/npolar.2015.056a61d1, 2015.

678
679 Inoue, H. Y. and Ishii M.: Variations and trends of CO₂ in the surface seawater in the
680 Southern Ocean south of Australia between 1969 and 2002, *Tellus, Ser. B*, 57, 58–69,
681 2005.
682
683 Jonas, T., Marty, C., and Magnusson, J.: Estimating the snow water equivalent from
684 snow depth measurements in the Swiss Alps, *J. Hydrol.*, 378, 161–167, 2009.
685
686 Kaleschke, L., Richter, A., Burrows, J., Afe, O., Heygster, G., and co-authors: Frost
687 flowers on sea ice as a source of sea salt and their influence on tropospheric halogen
688 chemistry, *Geophys. Res. Lett.*, 31, L16114, doi:10.1029/2004GL020655, 2004.
689
690 Kotovitch, M., Moreau, S., Zhou, J., Vancoppenolle, M., Dieckmann, G. S., and co-
691 authors: Air–ice carbon pathways inferred from a sea ice tank experiment, *Elementa:
692 Science of the Anthropocene*, 4, 1, doi10.12952/journal.elementa.000112, 2016.
693
694 Lindsay, R., and Schweiger, A.: Arctic sea ice thickness loss determined using
695 subsurface, aircraft, and satellite observations, *The Cryosphere*, 9(1), 269–283,
696 doi:10.5194/tc-9-269-2015, 2015.
697
698 Liss, P. S.: Processes of gas exchange across an air-water interface, *Deep-Sea Res.* 20,
699 221–238, 1973.
700
701 Massman, W., Sommerfeld, R., Zeller, K., Hehn, T., Hudnell, L., and Rochelle, S.: CO₂
702 flux through a Wyoming seasonal snowpack: diffusional and pressure pumping effects,
703 *Biogeochemistry of Seasonally Snow-Covered Catchments (Proceedings of a Boulder
704 Symposium, July 1995)*. IAHS Publ., 228, 71–79, 1995.
705
706 Massom, R.A., Eicken, H., Haas, C., Jeffries, M. O., Drinkwater, M. R., and other co-
707 authors: Snow on Antarctic sea ice, *Reviews of Geophysics*, 39, 413–445, 2001.
708

709 Mehrbach, C., Culbertson, C. H., Hawley, J. E., and Pytkowicz P. M.: Measurement of
710 the apparent dissociation constant of carbonic acid in seawater at atmospheric pressure,
711 *Limnol. Oceanogr.*, 18, 897–907, 1973.

712

713 Meier, W. N., Hovelsrud, G. K., van Oort, B. E. H., Key, J. R., Kovacs, K. M., and co-
714 authors: Arctic sea ice in transformation: A review of recent observed changes and
715 impacts on biology and human activity, *Rev. Geophys.*, 52, 185–217,
716 doi:10.1002/2013RG000431, 2014.

717

718 Miller, L. A., Papakyriakou, T. N., Collins, R. E., Deming, J. W., Ehn, J. K., and co-
719 authors: Carbon dynamics in sea ice: A winter flux time series, *J. Geophys. Res.*, 116,
720 C02028, doi:10.1029/2009JC006058, 2011.

721

722 Miller, L. A., Fripiat, F., Else, B. G. T., Bowman, J. S., Brown, K. A., and co-authors:.
723 Methods for Biogeochemical Studies of Sea Ice: The State of the Art, Caveats, and
724 Recommendation, *Elementa*, 3, 000038, doi:10.12952/journal.elementa.000038, 2015.

725

726 Nomura, D., Inoue, H. Y., and Toyota, T.: The effect of sea-ice growth on air–sea CO₂
727 flux in a tank experiment, *Tellus, Ser. B*, 58, 418–426, 2006.

728

729 Nomura, D., Inoue, H. Y., Toyota, T., and Shirasawa, K.: Effects of snow, snowmelting
730 and refreezing processes on air–sea-ice CO₂ flux, *J. Glaciol.*, 56, 196, 262–270, 2010a.

731

732 Nomura, D., Eicken, H., Gradinger, R., and Shirasawa, K.: Rapid physically driven
733 inversion of the air-sea ice CO₂ flux in the seasonal landfast ice off Barrow, Alaska
734 after onset of surface melt, *Cont. Shelf Res.*, 30, 1998–2004, 2010b.

735

736 Nomura, D., Granskog, M. A., Assmy, P., Simizu, D., and Hashida, G.: Arctic and
737 Antarctic sea ice acts as a sink for atmospheric CO₂ during periods of snow melt and
738 surface flooding, *J. Geophys. Res. Oceans*, 118, 6511–6524, 2013.

739

740 Merkouriadi, I., Gallet, J.-C., Graham, R. M., Liston, G. E., Polashenski, C., Rösel, A.,
741 and Gerland, S.: Winter snow conditions on Arctic sea ice north of Svalbard during the
742 Norwegian young sea ICE (N-ICE2015) expedition, *J. Geophys. Res. Atmos.*, 122,
743 doi:10.1002/2017JD026753, 2017.

744

745 Papadimitriou, S., Kennedy, H., Norman, L., Kennedy, D. P., Dieckmann, G. S., and
746 co-authors: The effect of biological activity, CaCO₃ mineral dynamics, and CO₂
747 degassing in the inorganic carbon cycle in sea ice in late winter-early spring in the
748 Weddell Sea, Antarctica, *J. Geophys. Res.* 117, C08011, doi:10.1029/2012JC008058,
749 2012.

750

751 Papakyriakou, T., and Miller, L. A.: Springtime CO₂ exchange over seasonal sea ice in
752 the Canadian Arctic Archipelago, *Ann. Glaciol.*, 52, 57, 215–224, 2011.

753

754 Parmentier, F. J. W., Christensen, T. R., Sørensen, L. L., Rysgaard, S., McGuire, A. D.,
755 and co-authors: The impact of lower sea-ice extent on Arctic greenhouse-gas exchange,
756 *Nature Climate Change*, 3, 195–202, doi:10.1038/nclimate1784, 2013.

757

758 Petrich, C. and Eicken, H.: Growth, structure and properties of sea ice, in Thomas, D. N.
759 and Dieckmann, G. S. eds., *Sea Ice*, 2nd ed., Oxford, Wiley-Blackwell, 23–77, 2010.

760

761 Pierrot, D., Lewis, E. and Wallace, D. W. R.: MS Excel Program Developed for CO₂
762 System Calculations, ORNL/CDIAC-105a. Carbon Dioxide Information Analysis
763 Center, Oak Ridge National Laboratory, U.S. Department of Energy, Oak Ridge,
764 Tennessee, doi: 10.3334/CDIAC/otg.CO2SYS_XLS_CDIA105a, 2006.

765

766 Powers, D., O'Neill, K., and Colbeck, S. C.: Theory of natural convection in snow, *J.*
767 *Geophys. Res.-Atmos.*, 90, 10641–10649, doi:10.1029/Jd090id06p10641, 1985.

768

769 Pringle, D. J., Miner, J. E., Eicken, H., and Golden, K. M.: Pore space percolation in sea
770 ice single crystals, *J. Geophys. Res.*, 114, C12017, doi:10.1029/2008JC005145, 2009.

771

772 Rysgaard, S., Søgaard, D. H., Cooper, M., Pucko, M., Lennert, K., and co-authors:
773 Ikaite crystal distribution in winter sea ice and implications for CO₂ system dynamics,
774 *The Cryosphere*, 7, 707–718, doi:10.5194/tc-7-707-2013, 2013.
775
776 Rösel, A., Itkin, P., King, J., Divine, D., Wang, C., Granskog, M. A., Krumpen, T. and
777 Gerland, S.: Thin Sea Ice, Thick Snow, and Widespread Negative Freeboard Observed
778 During N-ICE2015 North of Svalbard, *J. Geophys. Res. Oceans*, 123(2), 1156–1176,
779 doi:10.1002/2017JC012865, 2018.
780
781 Schindlbacher, A., Zechmeister-Boltenstern, S., Glatzel, G., and Jandl R.: Winter soil
782 respiration from an Austrian mountain forest, *Agric. For. Meteorol.*, 146, 205–215,
783 doi:10.1016/j.agrformet.2007.06.001, 2007.
784
785 Severinghaus, J. P., Albert, M. R., Courville, Z. R., Fahnestock, M. A., Kawamura, K.,
786 and co-authors: Deep air convection in the firn at a zero-accumulation site, central
787 Antarctica, *Earth Planet. Sci. Lett.*, 293, 359–367, doi:10.1016/J.Epsl.2010.03.003,
788 2010.
789
790 Stroeve, J. C., Serreze, M. C., Holland, M. M., Kay, J. E., Maslanik, J., and Barrett, A.
791 P.: The Arctic's rapidly shrinking sea ice cover: a research synthesis, *Climatic Change*,
792 110, 1005, doi:10.1007/s10584-011-0101-1, 2012.
793
794 Sørensen, L. L., Jensen, B., Glud, R. N., McGinnis, D. F., and Sejrt, M. K.:
795 Parameterization of atmosphere-surface exchange of CO₂ over sea ice, *The Cryosphere*,
796 8: 853–866. doi:10.5194/tc-8-853-2014, 2014.
797
798 Takagi, K., Nomura, M., Ashiya, D., Takahashi, H., Sasa, K., and co-authors: Dynamic
799 carbon dioxide exchange through snowpack by wind-driven mass transfer in a conifer-
800 broadleaf mixed forest in northernmost Japan, *Global Biogeochem. Cycles*, 19, GB2012,
801 doi:10.1029/2004GB002272, 2005.
802

803 Toyota, T., Massom, R., Tateyama, K., Tamura, T., and Fraser, A.: Properties of snow
804 overlying the sea ice off East Antarctica in late winter 2007, *Deep Sea Res. II*, 58,
805 1137–1148, 2011.

806

807 Vancoppenolle, M., Meiners, K. M., Michel, C., Bopp, L., Brabant, F., and co-authors:
808 Role of sea ice in global biogeochemical cycles: emerging views and challenges, *Quat.*
809 *Sci. Rev.*, 79, 207–230, 2013.

810

811 Weiss, R. F.: Carbon dioxide in water and seawater: the solubility of a non-ideal gas,
812 *Mar. Chem.*, 2, 203–215, 1974.

813

814 Zemmeling, H. J., Delille, B., Tison, J.-L., Hintsa, E. J., Houghton, L., and co-authors:.
815 CO₂ deposition over the multi-year ice of the western Weddell Sea, *Geophys. Res. Lett.*,
816 33, L13606, doi:10.1029/2006GL026320, 2006.

817

818 Zemmeling, H. J., Dacey, J. W. H., Houghton, L., Hintsa, E. J., and Liss, P. S.:
819 Dimethylsulfide emissions over the multi-year ice of the western Weddell Sea, *Geophys.*
820 *Res. Lett.*, 35, L06603, doi:10.1029/2007GL031847, 2008.

821

822 Zhou, J., Delille, B., Eicken, H., Vancoppenolle, M., Brabant, F., and co-authors:
823 Physical and biogeochemical properties in landfast sea ice (Barrow, Alaska): Insights
824 on brine and gas dynamics across seasons, *J. Geophys. Res.* 118, 6, 3172–3189, 2013.

825

826

827

828 **Figure captions**

829

830 Figure 1. Location map of the sampling area north of Svalbard during N-ICE2015.

831 Image of the sea ice concentrations (a) and station map (b) were derived from Special

832 Sensor Microwave Imager (SSM/I) satellite data for mean of February 2015 and from

833 Sentinel-1 (Synthetic Aperture Radar Sensor) satellite data, respectively.

834

835 Figure 2. Photographs of the CO₂ flux chamber system at station YI1 north of Svalbard
836 on Friday 13 March 2015. CO₂ flux chamber was installed over the frost flowers on the
837 new thin ice in the refreezing lead.

838

839 Figure 3. Example of the temporal variation in CO₂ concentration (ΔCO_2) in the
840 chambers installed at station YI1 that is use to calculate the CO₂ flux. ΔCO_2 indicates
841 the change in CO₂ concentration inside the chamber since the chamber was closed.

842

843 Figure 4. Time series of air temperature measured at the weather mast over the ice floe
844 (10 m height) (Hudson et al., 2015). Blank period indicates no data. Colored symbols
845 indicate the date for the chamber flux measurements. The horizontal dashed line
846 indicates air temperature = 0°C.

847

848 Figure 5. Vertical profiles of temperature (a) and salinity (b) in snow and sea ice (top 20
849 cm). The horizontal line indicates snow–ice interface. Shaded area indicates sea ice. The
850 triangle in (a) indicates the air temperature for each station. For stations FI7 and YI2
851 and 3, we have no salinity data.

852

853 Figure 6. Relationships between mean air–sea ice CO₂ fluxes and temperature
854 difference ($T_{\text{ice}} - T_{\text{a}}$) between ice (top 20 cm) (T_{ice}) and atmosphere (T_{a}) (circle) for F_{snow}
855 (blue), F_{ff} (black) and F_{ice} (red) for young and first-year sea ice. Relationships between
856 mean air–sea ice CO₂ fluxes and the difference of pCO₂ ($\Delta\text{pCO}_2_{\text{b-a}}$) between brine
857 (pCO_{2 b}) and atmosphere (pCO_{2 a}) (cross) for F_{snow} (blue) and F_{ice} (red).

858

859

860 **Table captions**

861

862 Table 1. Station, date for CO₂ flux measurement, position, floe number, surface
863 condition, ice type and thickness of snow, frost flowers, and sea ice.

864

865 a. Sea ice coring and snow sampling was conducted on 5 March 2015.

866

867 b. Sea ice coring and snow sampling was conducted on 10 March 2015.

868

869

870 Table 2. Station, snow density and water equivalent, brine volume fraction, and
871 temperature for sea ice (top 20 cm), brine temperature, salinity, DIC, TA, pCO₂ (pCO₂
872 b), and atmospheric temperature, wind speed, pCO₂ (pCO_{2 a})^a and ΔpCO_{2 b-a}.

873

874 a. pCO_{2 a} (μatm) was calculated from CO₂ concentration (ppmv) at Ny-Ålesund,
875 Svalbard (<http://www.esrl.noaa.gov/gmd/dv/iadv/>) taking into account saturated water
876 vapor and atmospheric pressure during sampling day.

877

878 b. Mean values for snow column.

879

880 c. "-" indicates no data. Due to logistical constraints, data of snow, sea ice, and brine
881 were not obtained.

882

883

884 Table 3. CO₂ flux measured over the snow (F_{snow}), frost flowers (F_{ff}), and ice surface
885 (F_{ice}). Values measured directly over undisturbed surfaces (either with frost flowers or
886 on snow surface) at a given station are indicated in bold.

887

888 a. Data of first CO₂ flux measurement after removal of snow or frost flowers.

889

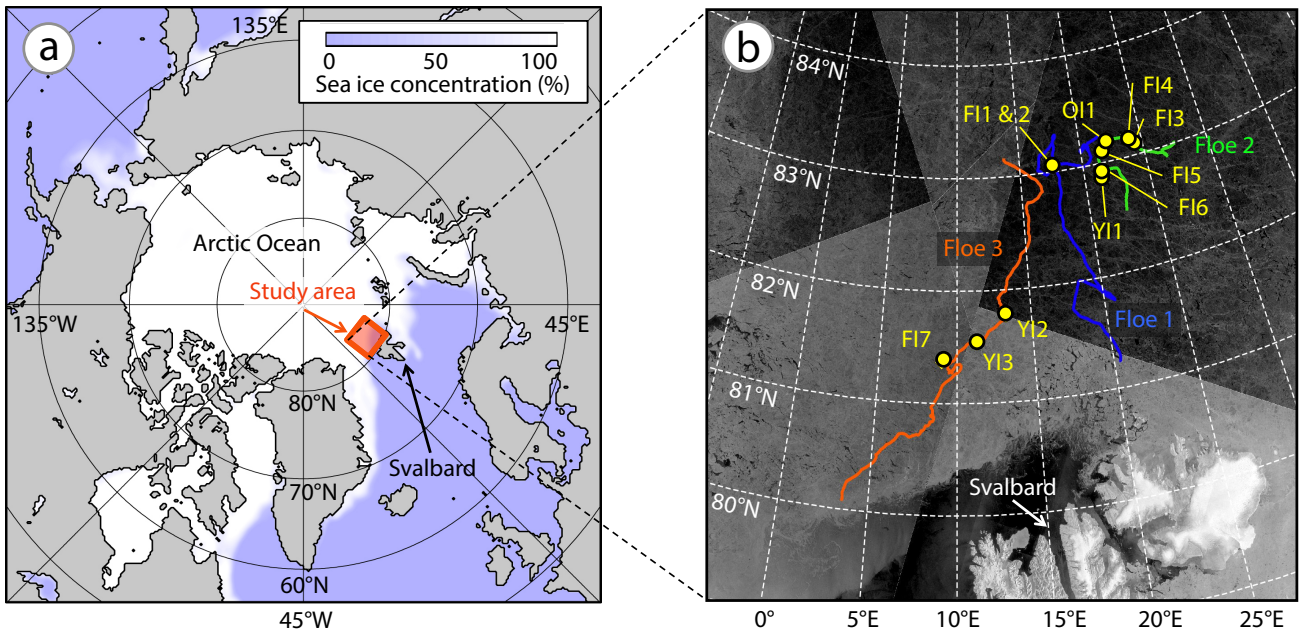
890 b. "-" indicates no data.

891

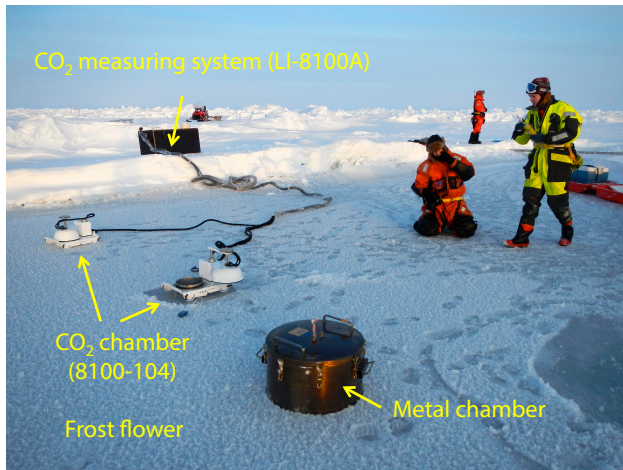
892 c. Number of measurements in bracket.

893

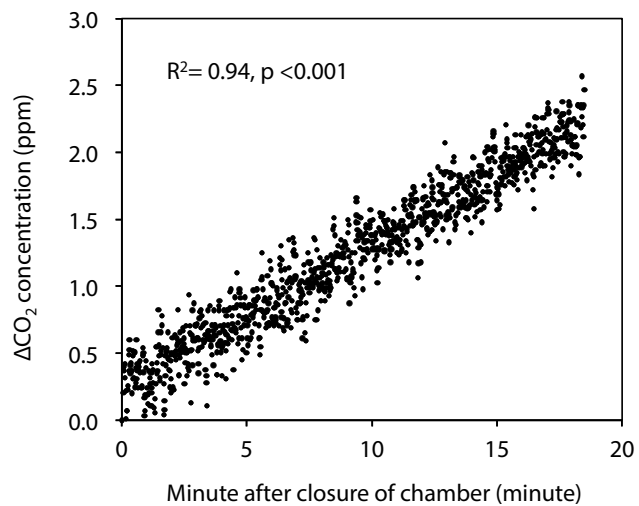
894 d. Data from station OI1 was not included.

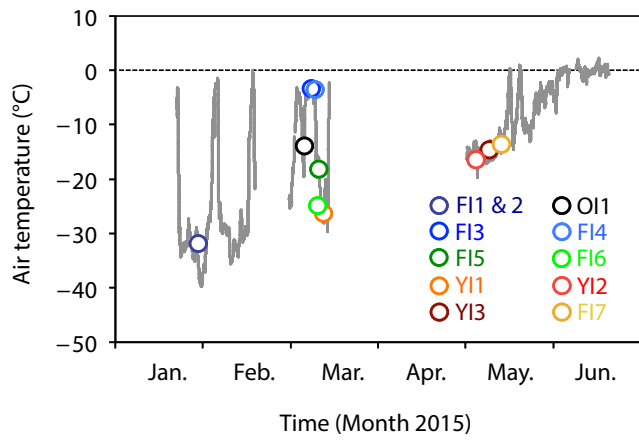


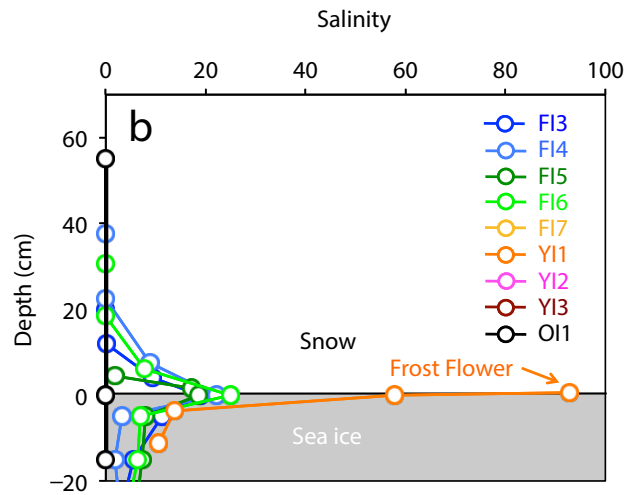
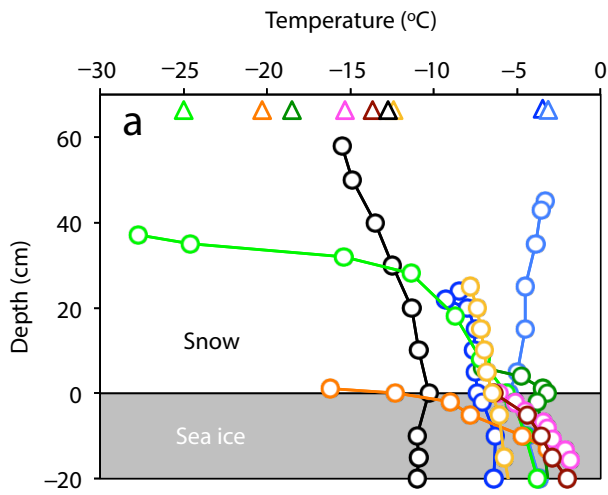
Nomura et al., Figure 1 (Double column size)



Nomura et al., Figure 2 (Single column size)







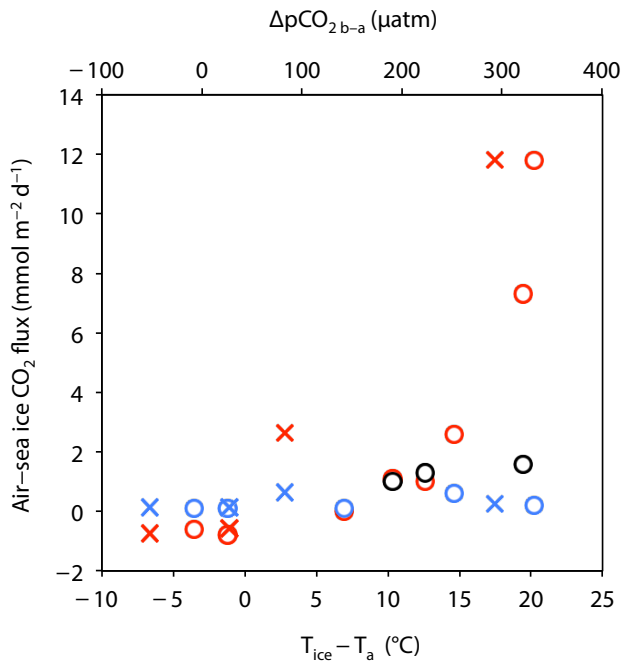


Table 1. Station, position, date for CO₂ flux measurement, floe number, surface condition, ice type and thickness of snow, frost flower, and sea ice.

Station	Position	Date of 2015	Floe number	Surface condition	Ice type ^c	Thickness (cm)		
						Snow	Frost flower	Sea ice
FI1	83°03.77N, 17°34.94E	28 January	1	Frost flower	First-year ice	0.0	1.0	37.0
FI2	83°03.77N, 17°34.94E	28 January	1	Snow	First-year ice	8.0	No	35.0
FI3	83°08.00N, 24°09.02E	5 and 8 March ^a	2	Snow	First-year ice	29.0	No	98.0
FI4	83°10.56N, 22°09.42E	9 March	2	Snow	First-year ice	36.0	No	92.0
FI5	83°06.02N, 21°38.29E	10 and 11 March ^b	2	Snow	First-year ice	3.0	No	48.0
FI6	82°55.36N, 21°25.92E	12 March	2	Snow	First-year ice	37.0	No	69.0
FI7	81°22.18N, 08°59.93E	13 May	3	Snow	First-year ice	26.5	No	127.0
YI1	82°52.52N, 21°16.54E	13 March	2	Frost flower	Young ice	0.0	1.0	15.0
YI2	81°46.53N, 13°16.00E	5 May	3	Snow and frost flower mixed	Young ice	2.5	2.5	17.5
YI3	81°32.45N, 11°17.20E	9 May	3	Snow and frost flower mixed	Young ice	2.0	2.0	22.0
OI1	83°07.18N, 24°25.59E	6 March	2	Snow	Old ice (multi-year ice)	60.0	No	>200

a. Sea ice coring, brine and snow sampling was conducted on 5 March 2015.

b. Sea ice coring, brine and snow sampling was conducted on 10 March 2015.

c. Ice type was categorized based on WMO (1970).

Table 2. Station, snow density and water equivalent, brine volume fraction and temperature for sea ice (top 20 cm), brine temperature, salinity, DIC, TA, pCO₂ (pCO_{2,b}) and atmospheric temperature, wind speed, pCO₂ (pCO_{2,a})^a and ΔpCO_{2,b-a}.

Station	Snow		Sea ice (top 20 cm)		Brine					Atmosphere				
	Density ^b (kg m ⁻³)	Water equivalent (kg m ⁻²)	Brine volume fraction (%)	Temperature (°C) (range)	Temperature (°C)	Salinity	DIC (μmol kg ⁻¹)	TA (μmol kg ⁻¹)	pCO _{2,b} (μatm)	Temperature (°C)	Wind speed (m second ⁻¹)	pCO _{2,a} (μatm)	ΔpCO _{2,b-a} (μatm)	
F11	— ^c	— ^c	— ^c	— ^c	— ^c	— ^c	— ^c	— ^c	— ^c	— ^c	—31.6	4.0	405	— ^c
F12	— ^c	— ^c	— ^c	— ^c	— ^c	— ^c	— ^c	— ^c	— ^c	— ^c	—31.6	4.0	405	— ^c
F13	399	104	9	-6.8 (-7.4 to -6.3)	-5.2	84.8	4628	5539	427	-3.3	9.0	400	27	
F14	400	180	9	-4.7 (-5.5 to -3.7)	-5.3	86.6	4433	5490	334	-3.5	6.2	386	-52	
F15	268	11	17	-3.5 (-3.8 to -3.1)	-3.3	51.8	3261	3518	472	-18.1	6.8	389	83	
F16	343	127	13	-4.8 (-5.7 to -3.8)	-4.8	84.0	4841	5493	693	-25.0	3.6	400	293	
F17	— ^c	— ^c	— ^c	-6.1 (-6.1 to -5.8)	— ^c	— ^c	— ^c	— ^c	— ^c	-13.0	5.8	405	— ^c	
Y11	— ^c	— ^c	17	-6.6 (-12.3 to -2.6)	— ^c	— ^c	— ^c	— ^c	— ^c	-26.0	2.6	402	— ^c	
Y12	— ^c	— ^c	— ^c	-3.6 (-5.1 to -1.8)	— ^c	— ^c	— ^c	— ^c	— ^c	-16.2	4.5	407	— ^c	
Y13	— ^c	— ^c	— ^c	-3.9 (-6.4 to -2.0)	— ^c	— ^c	— ^c	— ^c	— ^c	-14.2	6.7	410	— ^c	
OI1	— ^c	— ^c	0	-10.8 (-11.0 to -10.9)	— ^c	— ^c	— ^c	— ^c	— ^c	-13.5	4.7	397	— ^c	

a. pCO_{2,a} (μatm) was calculated from CO₂ concentration (ppmv) at Ny-Ålesund, Svalbard (<http://www.esrl.noaa.gov/gmd/dv/iadv/>) taking into account the saturated water vapor and atmospheric pressures at sampling day.

b. Mean values for column.

c. "—" indicates no data. Due to logistical constraints, data of snow, sea ice, and brine were not obtained.

Table 3. CO₂ flux measured over the snow (F_{snow}), frost flowers (F_{ff}) and ice surface (F_{ice}).

Station	CO ₂ flux (mmol C m ⁻² day ⁻¹)		
	Natural flux (mean ± 1SD)		Potential flux
	F _{snow}	F _{ff}	F _{ice} ^a
FI1	– ^b	+0.1 ± 0.1 (n=7) ^c	– ^b
FI2	+0.4 ± 0.3 (n=13) ^c	– ^b	– ^b
FI3	+0.1 ± 0.1 (n=7) ^c	– ^b	–0.6
FI4	+0.1 ± 0.1 (n=6) ^c	– ^b	–0.8
FI5	+0.6 ± 0.3 (n=5) ^c	– ^b	+2.6
FI6	+0.2 ± 0.1 (n=5) ^c	– ^b	+11.8
FI7	+0.1 ± 0.1 (n=10) ^c	– ^b	±0.0
YI1	– ^b	+1.6 ± 0.2 (n=6) ^c	+7.3
YI2	– ^b	+1.3 ± 0.2 (n=9) ^c	+1.0
YI3	– ^b	+1.0 ± 0.4 (n=8) ^c	+1.1
OI1	+0.1 ± 0.0 (n=6) ^c	– ^b	+0.2
Mean ^d	+0.2 ± 0.2 (n=46) ^c	+1.0 ± 0.6 (n=30) ^c	+2.5 ± 4.3 (n=9) ^c

a. Data of first measurement after removal of snow or frost flower.

b. "–" indicates no data.

c. Number of measurements in bracket.

d. Data of station OI1 was not included.